communications biology

Article

https://doi.org/10.1038/s42003-024-07377-x

Chemerin attenuates acute kidney injury by inhibiting ferroptosis via the AMPK/NRF2/SLC7A11 axis

Yidan Ma[1,2,5], Shengnan Fei[1,2,5], Xu Chen[1], Yuanyuan Gui[1,2], Bing Zhou[1,2], Tianya Xiang[1,2], Jianhang Liu[1], Kun Yue[1,2], Qingxin Li[1,2], Wei Jiang[3], Cheng Sun[4] & Xinzhong Huang[1]

Acute kidney injury (AKI) is a common and life-threatening condition associated with cell death, where ferroptosis plays a critical role. Chemerin, primarily produced in white adipose tissue, has multiple biological functions in renal pathophysiology. However, to date, whether and how chemerin regulates the progression of AKI remain unclear. Here, we found that chemerin expression was reduced in both AKI model mice and cells. Similarly, serum chemerin levels were also decreased in AKI patients. The administration of recombinant chemerin improves renal function in ischemia-reperfusion (I/R) model mice. Chemerin significantly attenuates ferroptosis in kidneys. In TCMK-1 cells, chemerin knockdown further aggravates ferroptosis. Mechanistically, chemerin activates AMP-activated protein kinase (AMPK), which induces the phosphorylation of nuclear factor erythroid 2-related factor 2 (NRF2) in renal tubular cells. Subsequently, NRF2 translocates into the nucleus, where it stimulates the expression of cystine/glutamate antiporter solute carrier (SLC7A11). As a result, cystine uptake and glutathione (GSH) biosynthesis in renal tubular cells were increased, which confers cells with higher capacity against ferroptosis. Overall, our findings indicate that chemerin plays a protective role in AKI by repressing ferroptosis in renal tubular cells, which is likely due to the activation in the AMPK/NRF2/SLC7A11 axis.

Acute kidney injury (AKI) is commonly caused by renal ischemia-reperfusion (I/R) injury, sepsis, trauma, and renal transplantation, making it a prevalent disorder with high morbidity and mortality[1,2]. AKI has been identified as a risk factor for the development of chronic kidney disease (CKD) or end-stage renal disease (ESRD). Approximately 30% of AKI patients eventually progress to CKD or ESRD[3–5]. As the fundamental structural units of the kidney, renal tubular cells are crucial for maintaining proper kidney function, including metabolic processing to reabsorption. However, renal tubular cells are highly susceptible to various harmful stimuli and play a central role in the pathophysiology of AKI. Hence, renal tubular cell death, through apoptosis, necrosis, and pyroptosis, is a hallmark of AKI[6]. Recently, increasing evidence has indicated that ferroptosis in renal tubular cells contributes to the progression of AKI[7–9]. Therefore, studies aimed at deepening our understanding of renal tubular cell ferroptosis are critical for developing effective strategies to combat AKI[10,11].

Chemerin, a multifunctional adipokine encoded by *retinoic acid responder 2* (RARRES2) and *Tazarotene induced gene 2* (TIG2), is secreted by various cells, including adipocytes, epithelial, and endothelial cells[12]. Several proteins, such as CC chemokine-like receptor 2 (CCRL2), G protein-coupled receptor 1 (GPR1), and chemokine-like receptor 1 (CMKLR1), have been identified as chemerin receptors and are ubiquitously expressed in most tissues[13]. In renal diseases, chemerin has been shown to attenuate CKD by inhibiting vascular calcification[14], and certain chemerin variants have been identified as risk factors for diabetic nephropathy[15]. However, the role of chemerin in AKI remains unclear. A recent study showed that chemerin inhibits fatty acid oxidation and ameliorates ferroptosis in cancer cells[16]. Given the importance of ferroptosis in the progression of AKI, we hypothesized that chemerin may play a beneficial role in AKI by inhibiting ferroptosis in renal tubular cells.

[1]Department of Nephrology, Affiliated Hospital of Nantong University, 20 Xisi Road, Nantong, 226001 Jiangsu, China. [2]Medical School of Nantong University, Nantong, 226001 Jiangsu, China. [3]Department of Emergency Medicine, Affiliated Hospital of Nantong University, Nantong, 226001 Jiangsu, China. [4]Key Laboratory of Neuroregeneration of Jiangsu and Ministry of Education, NMPA Key Laboratory of Research and Evaluation of Tissue Engineering Technology Products, School of Medicine, Nantong University, Nantong, 226001 Jiangsu, China. [5]These authors contributed equally: Yidan Ma, Shengnan Fei.
e-mail: huangxz421@126.com

In this study, we examined the potential role of chemerin in AKI. Our data showed that chemerin expression was reduced in AKI model cells, mice, and patients. The application of recombinant chemerin protected TCMK-1 cells from erastin-induced ferroptosis. Moreover, chemerin treatment markedly attenuated renal failure in I/R model mice. Mechanistically, chemerin activated AMPK in renal tubular cells, leading to

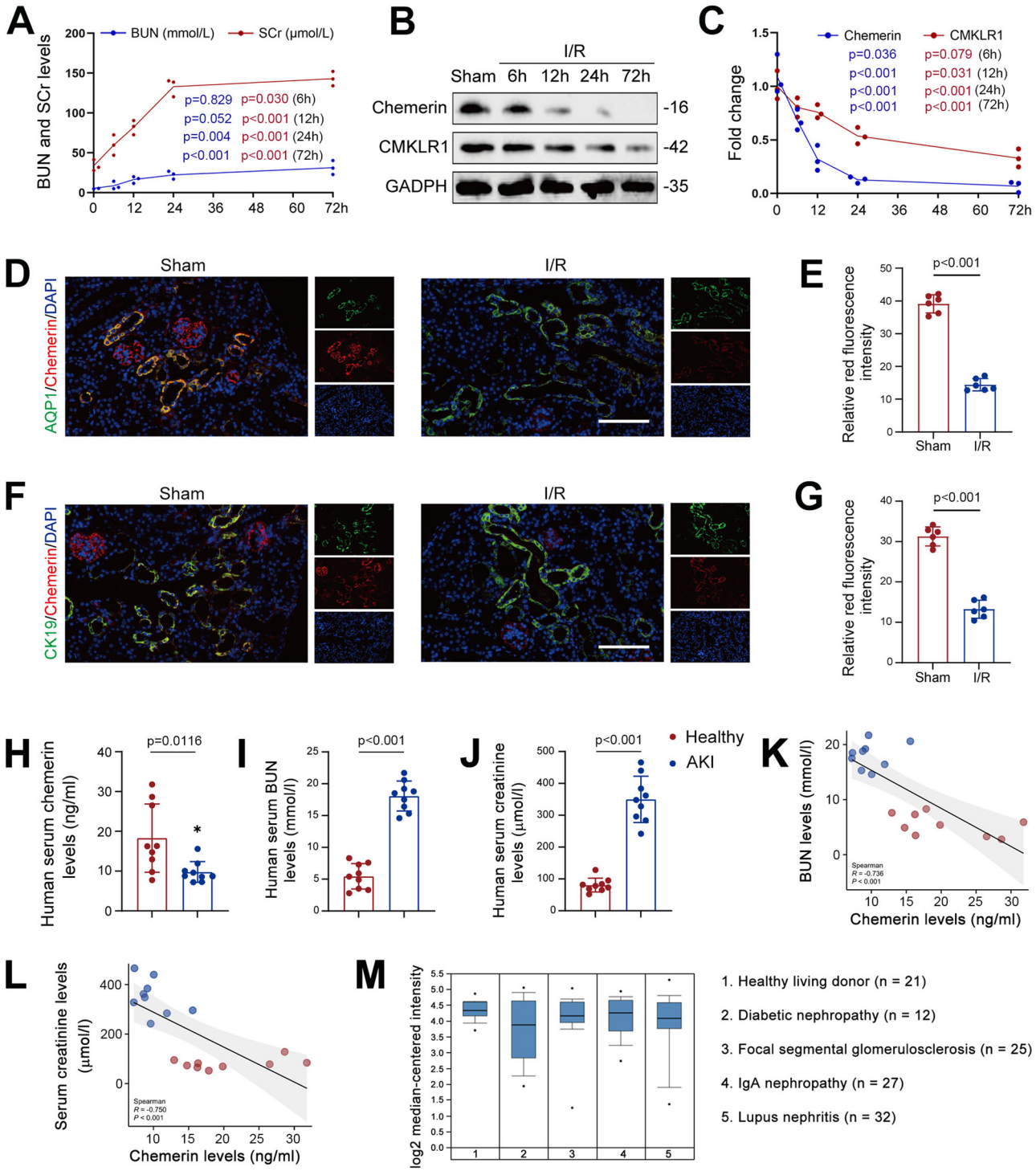

Fig. 1 | Chemerin expression is reduced in AKI. A Serum creatinine (SCr) and blood urea nitrogen (BUN) levels continuously increased in I/R model mice. $n = 6$ mice/group. **B** Temporal expression patterns of chemerin and CMKLR1 in the kidneys of I/R model mice. $n = 3$ (independent experiments). **C** Quantified data for chemerin and CMKLR1 from the western blots shown in (**B**). **D**–**G** Immunofluorescence analysis of chemerin (red; **D**, **F**) expression in the renal cortices. Relative immunofluorescence intensities for chemerin are presented in (**E**) and (**G**), respectively. AQP1 (green; **D**) and CK19 (green; **F**) were used as markers for renal tubular epithelial cells, and DAPI (blue) was used to stain the nuclei. Scale bar = 100 μm. $n = 6$ mice/group. Serum chemerin (**H**), blood urea nitrogen (BUN; **I**), and creatinine (**J**) levels in healthy individuals and AKI patients. $n = 9$ humans/group. Spearman correlation analysis between serum chemerin and BUN (**K**) or creatinine (**L**). $n = 9$ humans/group. **M** Chemerin expression decreased in nephropathy patients. Data analysis from Nephroseq database (https://www.nephroseq.org). Data are presented as the mean ± SD, $^{*}p < 0.05$, $^{**}p < 0.01$, $^{***}p < 0.001$. One-way ANOVA with Tukey's multiple comparison test was used for (**A**) and (**C**), Student's *t* test was used for (**E**), (**G**)–(**J**).

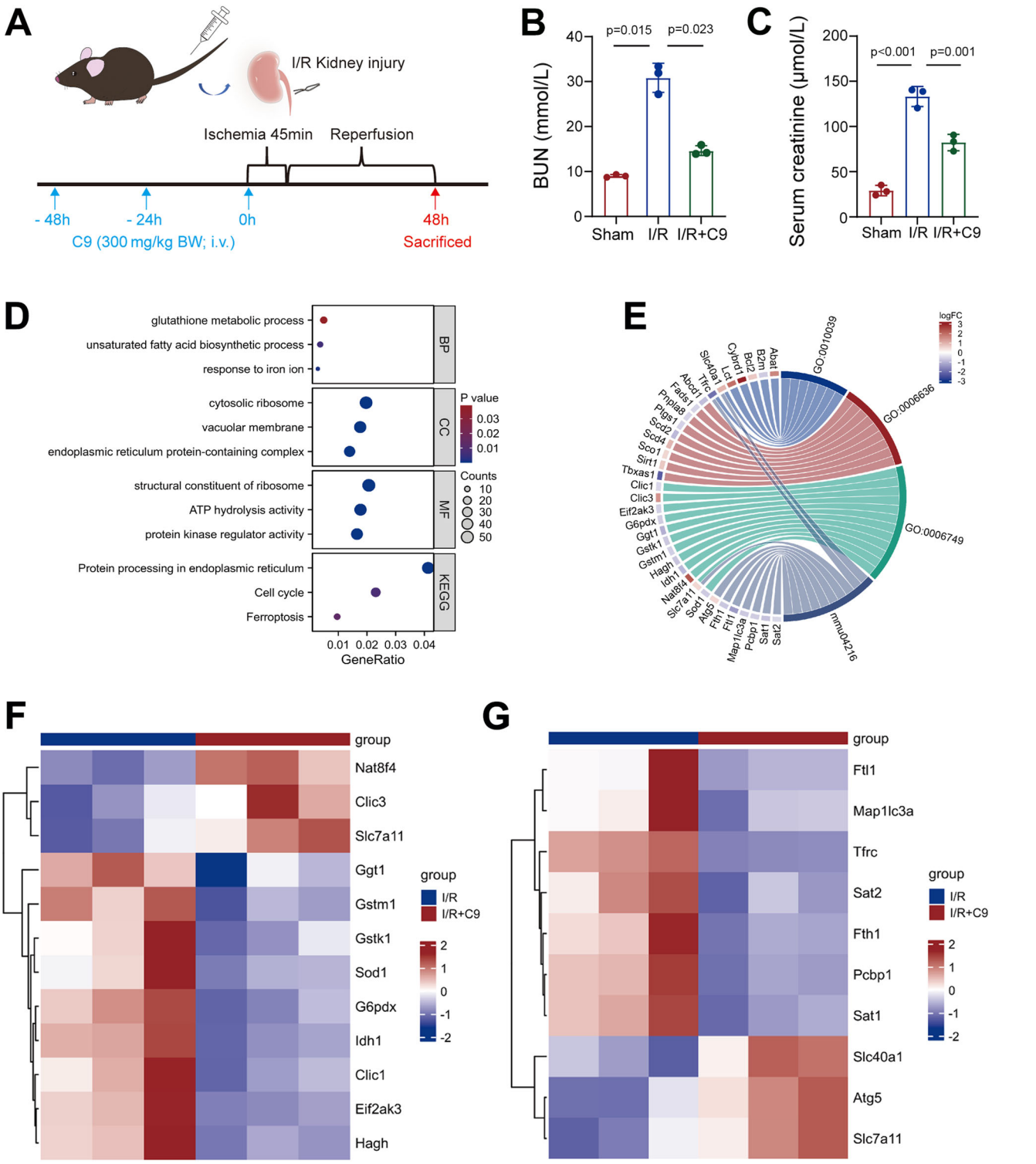

Fig. 2 | Chemerin reduces renal injury in I/R model mice by affecting ferroptosis. **A** Experimental scheme. Mice were intravenously (i.v.) injected with recombinant chemerin-9 (C9) at a dose of 300 mg/kg body weight (BW), administered 3 times as indicated. Simultaneously, the mice underwent I/R surgery. Forty-eight hours post-surgery, the mice were sacrificed for further analysis. C9 treatment reduces blood urea nitrogen (BUN; **B**) and serum creatinine (**C**) levels. $n = 3$ mice/group. **D** GO and KEGG analyses for differentially expressed genes. BP biological process, CC cellular component, MF molecular function, KEGG Kyoto encyclopedia of genes and genomes. **E** Chord diagram of differentially expressed genes. Kidney samples were subjected to RNA-Seq analysis. GO:0010039 represents the cluster of response to iron ion. GO:0006636 represents the cluster of unsaturated fatty acid biosynthetic process. GO:0006749 represents the cluster of glutathione metabolic process. mmu04216 represents the cluster of ferroptosis. Heatmap for differentially expressed genes involved in glutathione metabolic process (**F**) and ferroptosis (**G**). Data are presented as the mean ± SD, $^{*}p < 0.05$, $^{**}p < 0.01$, $^{***}p < 0.001$, by one-way ANOVA with Tukey's multiple comparison test.

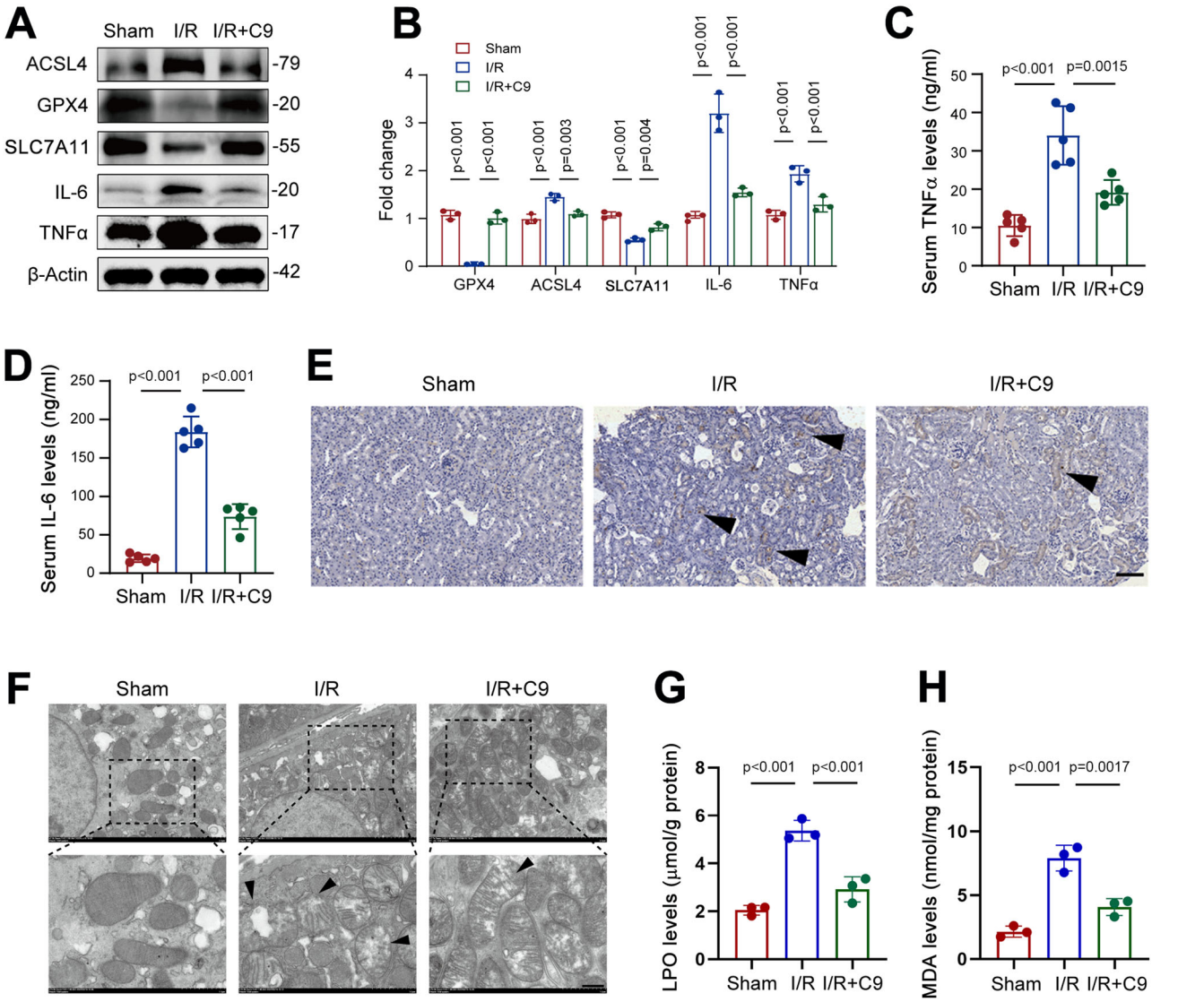

Fig. 3 | Chemerin-9 alleviates ferroptosis in the kidney to attenuate renal I/R injury. **A** Western blot analysis of GPX4, ACSL4, SLC7A11, IL-6, and TNFα abundance in the kidneys. β-Actin was used as a loading control. $n = 3$ (independent experiments). **B** Quantified data from the western blots shown in (**A**). **C**, **D** Serum TNFα (**C**) and IL-6 (**D**) levels were reduced by C9 in I/R model mice. $n = 5$ mice/group. **E** Representative Prussian blue staining images showing iron deposition in the kidneys. Arrows indicate positive signals for iron staining. Scale bars = 100 μm. **F** Representative transmission electron microscopy (TEM) images showing mitochondrial structures in the kidneys. Arrows indicate damaged mitochondria. Scale bars = 5 μm. Lipid hydroperoxide (LPO; **G**) and malondialdehyde (MDA; **H**) levels were decreased by C9. $n = 3$ mice/group. Data are presented as the mean ± SD, $^{*}p < 0.05$, $^{**}p < 0.01$, $^{***}p < 0.001$, by one-way ANOVA with Tukey's multiple comparison test.

increased phosphorylation of NRF2 (p-NRF2). Once phosphorylated, NRF2 translocated into the nucleus, where it stimulated the transcription of SLC7A11. This facilitated cysteine uptake into renal tubular cells, enhancing GSH synthesis, which conferred cells with higher capacity to combat ferroptosis. In this way, chemerin plays a protective role in AKI and may serve as a potential therapeutic target for treating the condition.

Results

Chemerin was reduced in AKI

To explore the potential role of chemerin in AKI, we first analyzed its expression in I/R model mice. As shown in Fig. 1A, serum creatinine (SCr) and blood urea nitrogen (BUN) levels continuously increased up to 72 h post-surgery, indicating impaired renal function in these I/R mice. Meanwhile, we found that chemerin and its receptor CMKLR1 expression in the kidneys decreased over time following I/R surgery (Fig. 1B, C). Similar changes in chemerin and CMKLR1 in the kidney were observed in other AKI mouse models induced by cisplatin or LPS (Supplementary Fig. 1A, B). Immunofluorescence analysis further confirmed the reduction of chemerin in the kidneys of I/R mice (Fig. 1D–G and Supplementary Fig. 1C, D). In the AKI cell model, chemerin expression was decreased in H_2O_2-treated TCMK-1 cells (Supplementary Fig. 1E, F), a trend that was further validated by immunofluorescence analysis (Supplementary Fig. 1G, H). Notably, chemerin co-localized with AQP1 and CK19, indicating its expression in renal tubular epithelial cells (Fig. 1D, F). Most importantly, serum chemerin levels were also reduced in AKI patients (Fig. 1H). Moreover, serum chemerin levels were reversely correlated with serum BUN and creatinine levels (Fig. 1I–L). Accordingly, data from the Nephroseq database showed that chemerin expression was reduced in the kidney in various renal diseases (Fig. 1M). These findings strongly suggest that chemerin plays a role in the progression of AKI.

Chemerin represses ferroptosis to alleviate renal I/R injury

Next, we asked whether chemerin administration could attenuate AKI. To test this, we administered recombinant truncated chemerin with 9 amino

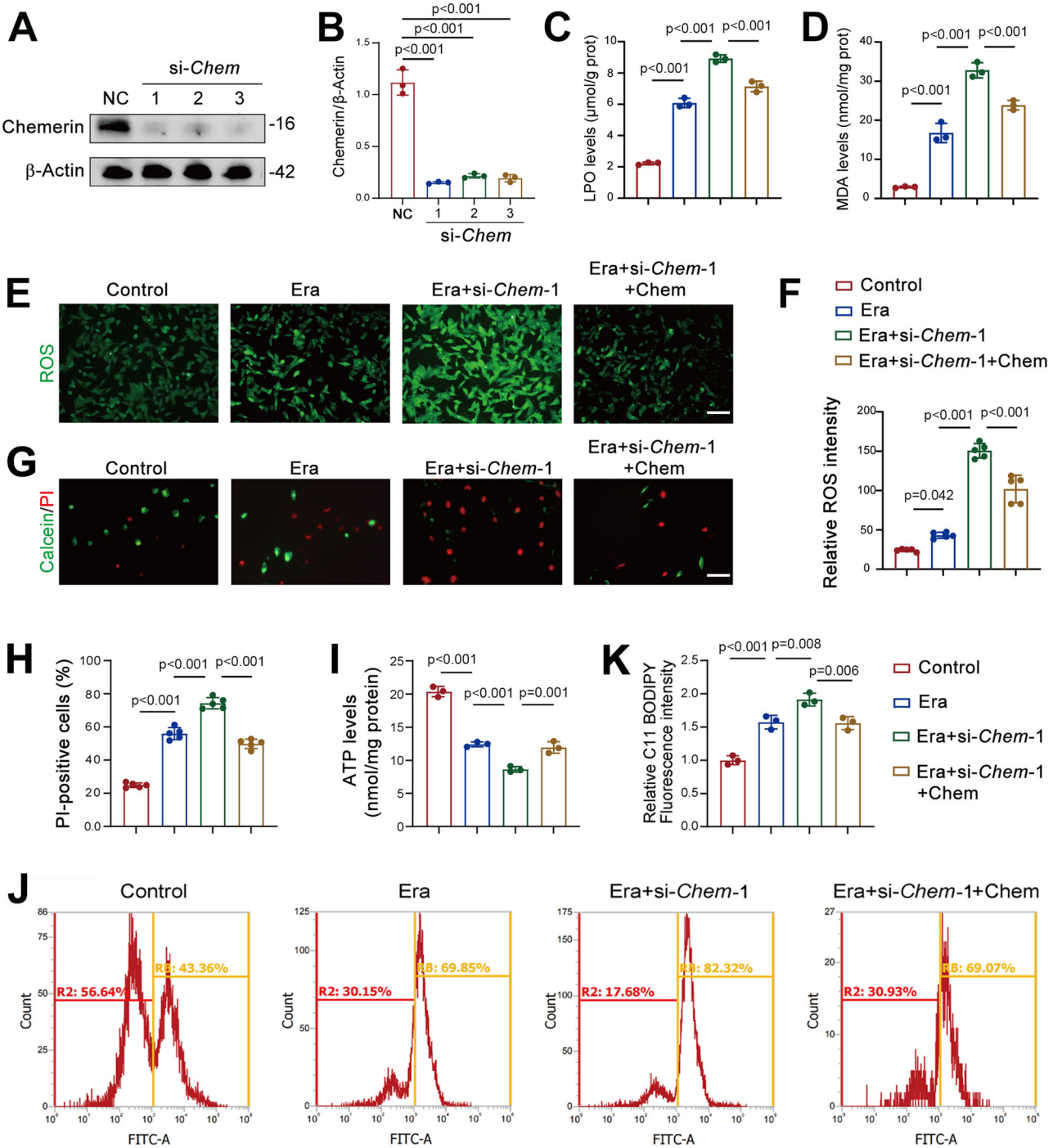

Fig. 4 | Chemerin knockdown exacerbates ferroptosis in renal tubular cells. **A** Western blot analysis showing the efficiency of chemerin knockdown. TCMK-1 cells were transfected with siRNA targets *Chem* (si-*Chem*). Seventy-two hours post-transfection, cells were harvested for western blot analysis. β-Actin was used as a loading control. $n = 3$ (independent experiments). **B** Quantified data from the western blots shown in (**A**). Recombinant chemerin counteracts the increases in lipid hydroperoxide (LPO; **C**) and malondialdehyde (MDA; **D**) levels induced by chemerin knockdown. TCMK-1 cells were transfected with si-*Chem*-1. Forty-eight hours post-transfection, cells were treated with recombinant chemerin (20 ng/ml) and erastin (Era, 5 μM) for additional 24 h. $n = 3$ (independent experiments). **E** Representative images showing reactive oxygen species (ROS). Cell treatments were described as in (**C**, **D**). $n = 5$ (independent experiments). Scale bar = 50 μm. **F** Quantified relative immunofluorescence intensity as shown in (**E**). **G** Calcein/PI staining showing live and dead cells. Cell treatments were described as in (**C**, **D**). $n = 5$ (independent experiments). Scale bar = 100 μm. **H** Quantified PI-positive cells from the calcein/PI staining in (**G**). **I** ATP levels. Cell treatments were described as in (**C**, **D**). $n = 3$ (independent experiments). **J** Lipid peroxidation. Oxidized lipids were captured by using C11 BODIPY and assayed by flow cytometry. Cell treatments were described as in (**C**, **D**). $n = 3$ (independent experiments). **K** Quantified lipid peroxidation from the flow cytometry in (**J**). Data are presented as the mean ± SD. $^{**}p < 0.01$ and $^{***}p < 0.001$, by one-way ANOVA with Tukey's multiple comparison test.

acids (C9) to I/R model mice and assessed renal function (Fig. 2A). As expected, C9 treatment significantly reduced the elevations in blood urea nitrogen (BUN) and serum creatinine levels caused by I/R injury (Fig. 2B, C). Consistent with these improvements, periodic acid-Schiff (PAS) staining showed that C9 attenuated tubular injury in the I/R model mice (Supplementary Fig. 2A, B). To explore the underlying mechanisms, we conducted RNA sequencing (RNA-Seq), which identified 3103 differentially expressed genes in the kidney. Of these, 1605 were up-regulated and

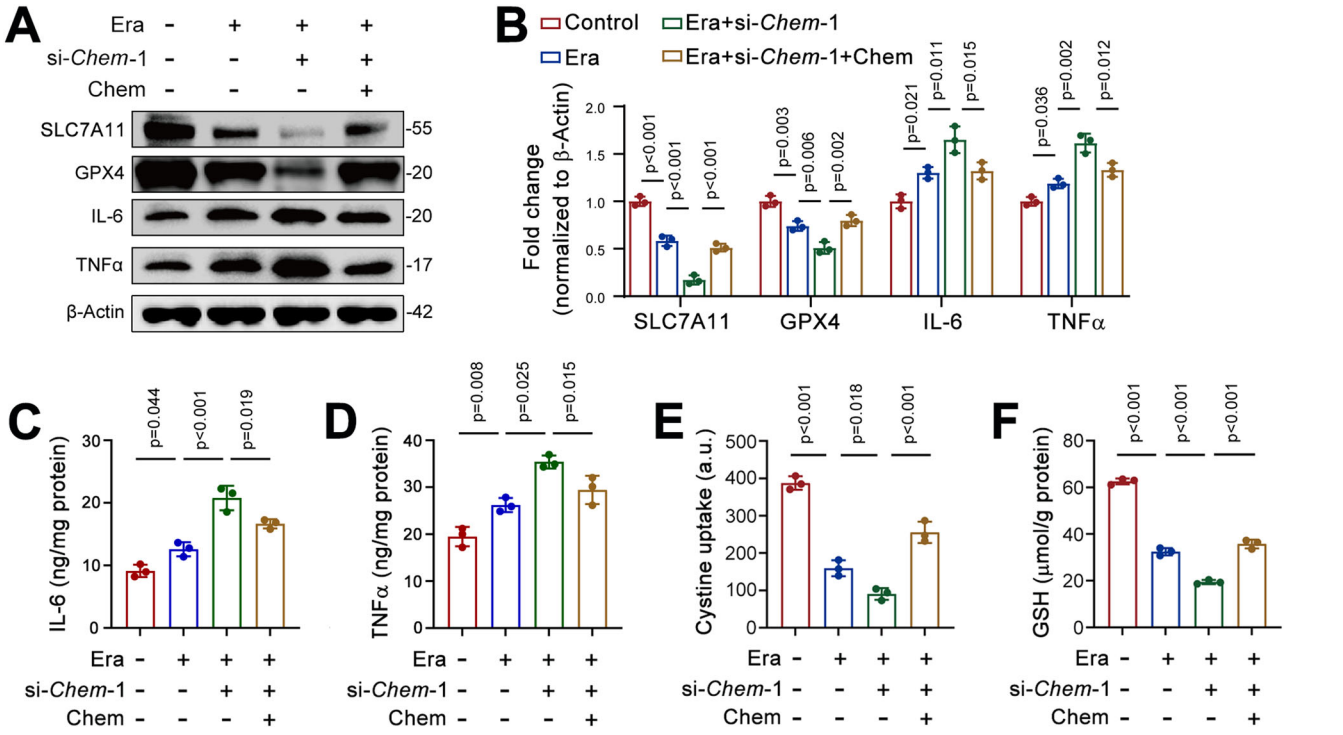

Fig. 5 | Chemerin knockdown aggravates ferroptosis in renal tubular epithelial cells. A Recombinant chemerin reverses changes in SLC7A11, IL-6, and TNFα expression induced by chemerin knockdown. TCMK-1 cells were transfected with si-*Chem*-1. Forty-eight hours post-transfection, cells were treated with recombinant chemerin (20 ng/ml) and erastin (Era, 5 μM) for additional 24 h. Protein expression was analyzed by western blot, with β-Actin used as a loading control. $n = 3$ (independent experiments). **B** The quantified data for the western blots as shown in (**A**). IL-6 (**C**), TNFα (**D**), Cystine uptake (**E**), and GSH levels (**F**) levels in TCMK-1 cells treated with si-*Chem*-1 and recombinant chemerin. The treatment conditions were described in (**A**). $n = 3$ (independent experiments). Data are presented as the mean ± SD, $^{*}p < 0.05$, $^{**}p < 0.01$, and $^{***}p < 0.001$, by one-way ANOVA with Tukey's multiple comparison test.

1498 were down-regulated (Supplementary Data 1). Gene ontology (GO) and KEGG pathway analysis revealed that these genes are closely associated with ferroptosis, as evidenced by clusters related to glutathione metabolic process, unsaturated fatty acid biosynthetic process, response to iron ion, and ferroptosis (Fig. 2D). A chord diagram illustrated the connections between differentially expressed genes in these four clusters (Fig. 2E). Notably, *Slc7a11* was implicated in both the glutathione metabolic process and ferroptosis clusters (Fig. 2E). Heatmaps of differentially expressed genes within these pathways further confirmed that *Slc7a11* was up-regulated by C9 treatment (Fig. 2F, G). Based on these RNA-Seq data and bioinformatics analyses, we propose that ferroptosis plays a role in nephroprotective effects of chemerin, with *Slc7a11* serving as a key factor.

To address this speculation as aforementioned, we analyzed expression of ferroptosis-related proteins. Our results showed that ACSL4 levels progressively increased following I/R surgery, while GPX4 displayed an opposite trend (Supplementary Fig. 2C, D). Notably, the increase in ACSL4, along with the decreases in GPX4 and SLC7A11 observed in I/R mice, were reversed by C9 treatment (Fig. 3A, B). Immunofluorescence analysis also confirmed that the reductions in GPX4 and SLC7A11 in the kidneys of I/R mice were mitigated by C9 (Supplementary Fig. 3A–D). These findings indicate that the enhanced ferroptosis seen in the kidney of I/R mice was attenuated by C9. Since inflammation is a common feature of ferroptosis, driven by excessive lipid peroxidation and reactive oxygen species (ROS)[17,18], we further examined the expression of IL-6 and TNFα. Our data showed that C9 treatment reduced IL-6 and TNFα levels in the kidneys of I/R mice (Fig. 3A, B), and these changes were confirmed by immunofluorescence (Supplementary Fig. 3E–H). Additionally, serum levels of IL-6 and TNFα were also decreased in C9-treated mice (Fig. 3C, D). Prussian blue staining indicated increased iron deposition in renal tubular cells following I/R, but C9 treatment mitigated this effect (Fig. 3E). Furthermore, transmission electron microscopy (TEM) analysis of kidney mitochondria showed that disrupted cristae were prevalent in I/R mice, while C9 treatment significantly reduced the number of damaged mitochondria (Fig. 3F). Additionally, lipid hydroperoxide (LPO) and malondialdehyde (MDA) levels, which were elevated by I/R, were abolished by C9 treatment (Fig. 3G, H). Collectively, these data indicate that chemerin plays a beneficial role in AKI, likely by reducing ferroptosis in the kidney.

Chemerin knockdown worsens ferroptosis in renal tubular cells

To further validate the protective role of chemerin in AKI, we examined whether chemerin knockdown affects ferroptosis in renal tubular cells. Chemerin expression was significantly reduced by siRNAs targeting the *Chemerin* gene (si-*Chem*-1, -2, and -3) in TCMK-1 cells (Fig. 4A, B). Erastin-induced increases in LPO and MDA levels were further exacerbated by si-*Chem*-1 (Fig. 4C, D). Notably, the application of chemerin partially counteracted these increases in LPO and MDA (Fig. 4C, D). Similar patterns were observed in reactive oxygen species (ROS) production in TCMK-1 cells (Fig. 4E, F). Erastin-induced cell death was further increased by si-*Chem*-1, and chemerin application attenuated this increase (Fig. 4G, H). Chemerin knockdown also caused a reduction in ATP levels, which was prevented by the application of chemerin (Fig. 4I). Additionally, the enhanced lipid peroxidation induced by si-*Chem*-1 was mitigated by chemerin (Fig. 4J, K). The findings regarding ATP levels and lipid peroxidation were further validated using si-*Chem*-3 (Supplementary Fig. 4A–C).

We next examined ferroptosis-related protein expression cells treated with si-*Chem*-1. Western blot analysis revealed that SLC7A11 and GPX4 levels were decreased by erastin, and these reductions was further aggravated by chemerin knockdown (Fig. 5A, B). Exogenous chemerin restored SLC7A11 and GPX4 levels in cells treated with both erastin and si-*Chem*-1 (Fig. 5A, B). Similarly, erastin treatment increased IL-6 and TNFα expression, and chemerin knockdown further amplified these effects (Fig. 5A, B). Exogenous chemerin reversed the elevated IL-6 and TNFα levels in erastin

and si-*Chem*-1 treated cells (Fig. 5A, B). These changes were reflected in serum IL-6 and TNFα levels (Fig. 5C, D). Immunofluorescence data further corroborated these findings for SLC7A11, GPX4, IL-6, and TNFα (Supplementary Fig. 5A–G). TCMK-1 cells express the chemerin receptor CMKLR1 (Supplementary Fig. 6A). Similar to chemerin, chemerin-9 (C9) exhibited anti-ferroptotic activity in erastin-treated TCMK-1 cells, as evidenced by reduced ACSL4 and increased GPX4 levels (Supplementary Fig. 6B, C). Additionally, the erastin-induced increases in IL-6 and TNFα were also prevented by C9 (Supplementary Fig. 6B, C). Cystine uptake and GSH levels followed a similar pattern of changes as SLC7A11 (Fig. 5E, F). Together, these loss-of-function studies further confirm the beneficial role of chemerin in AKI.

Chemerin alleviates ferroptosis by upregulating SLC7A11 in renal tubular cells

We next sought to elucidate the mechanism underlying the observed beneficial effects of chemerin in AKI. As previously noted, chemerin induced SLC7A11 expression in renal tubular cells, while chemerin knockdown suppressed its expression. Given the critical role of SLC7A11 in ferroptosis[19–21], together with our RNA-Seq data, we hypothesized that chemerin improves renal function in AKI by upregulating SLC7A11 expression. To test this hypothesis, we knocked down SLC7A11 in TCMK-1 cells using si-*SLC*-1, -2, and -3 (Fig. 6A, B). SLC7A11 knockdown significantly diminished the protective effects of chemerin in erastin-induced ferroptosis, as showed by reduced GPX4 levels and increased ACSL4 expression (Fig. 6C, D). These alterations in GPX4 and ACSL4 were corroborated by immunofluorescence data (Supplementary Fig. 6D–G). The reduced ROS production observed in chemerin-treated cells was reversed by si-*SLC*-1 (Fig. 6E, F), and the repressed cell death and improved ATP levels were similarly counteracted by SLC7A11 knockdown (Fig. 6G–I). Oxidized lipids were decreased by chemerin in erastin-treated cells, which was reversed by si-*SLC*-1 (Fig. 6J, K). These observed changes in ATP and oxidized lipid levels were recapitulated by SLC7A11 knockdown using si-*SLC*-2 (Supplementary Fig. 7A–C). Likewise, the reduced LPO and MDA levels by chemerin were reversed by SLC7A11 knockdown (Fig. 6L, M). Moreover, chemerin-induced increase in cystine uptake and GSH production in erastin-treated cells were also negated by SLC7A11 knockdown (Fig. 6N, O). These findings suggest that chemerin protects renal function in AKI by upregulating SLC7A11 expression in renal tubular cells.

Chemerin targets AMPK/NRF2 pathway to enhance SCL7A11 expression

AMPK activation has been shown to attenuate ferroptosis in various cell types, including hepatocytes[22], intestinal epithelial cells[23], cancer cells[24], and oligodendrocyte progenitor cells[25]. Therefore, we hypothesized that AMPK plays a central role in mediating the protective effects of chemerin in AKI. To test this, we treated TCMK-1 cells with chemerin and AMPK inhibitor dorsomorphin (Dor) and measured phosphorylated AMPK (p-AMPK). Our results showed that chemerin increased p-AMPK levels, an effect that was negated by Dor (Fig. 7A, B). NRF2, a downstream substrate of AMPK, is known to regulate ferroptosis[26–28]. Once activated, NRF2 translocates into the nucleus, where it functions as a transcriptional factor to upregulate downstream genes[29], including *Slc7a11*[30–32]. Since chemerin also regulates SLC7A11, we investigated whether NRF2 is involved in transducing the renal protective effects of chemerin in AKI. Chemerin treatment increased phosphorylated NRF2 (p-NRF2), and AMPK inhibition by Dor reversed this effect (Fig. 7A, B). Similarly, to NRF2, chemerin-induced SLC7A11 expression was also blocked by Dor (Fig. 7A, B). These changes in p-NRF2 and SLC7A11 were further confirmed by immunofluorescence analysis (Fig. 7C–F). In line with these findings, chemerin-induced increases in cystine uptake and GSH synthesis were inhibited by Dor (Fig. 7G, H). To further validate these results, we used ML385, a potent inhibitor of NRF2. Chemerin-induced increases in p-NRF2 levels in the nucleus were significantly reduced by ML385 (Fig. 8A, B). Immunofluorescence analysis further confirmed these changes in NRF2 distribution (Fig. 8C, D). Similarly, chemerin-induced SLC7A11 expression was diminished by ML385 (Fig. 8F, G), and the associated increases in cysteine uptake and GSH production were also reversed (Fig. 8H, I). Moreover, we also analyzed the AMPK/NRF2 axis in vivo. The results showed that p-AMPK levels were reduced in the kidneys of I/R mice, but this decline was prevented by C9 treatment (Supplementary Fig. 8A, B). Similarly, p-NRF2 exhibited parallel changes, with its reduction in I/R mice being counteracted by C9 treatment (Supplementary Fig. 8A, B). Collectively, these findings suggest that chemerin attenuates renal injury in AKI by activating the AMPK/NRF2/SLC7A11 signaling axis.

Discussion

White adipose tissue is a specialized type of loose connective tissue primary composed of adipocytes. The primary function of adipocytes is to store fat and release fatty acids to supply energy to the body. Recent studies have shown that white adipose tissue can secret a wide range of hormones, potentially making it the largest endocrine tissue in the body[33]. It is well established that obesity is causative factor for several detrimental outcomes, such as metabolic syndromes, cardiovascular diseases, and cancers. However, a growing body of evidence suggests that overweight and obese patients often have better clinical outcomes after critical illness, a phenomenon known as "obesity paradox"[34]. In the context of nephropathy, Peter Stenvinkel et al. observed a protective effect of high body mass index (BMI) in patients undergoing hemodialysis[35]. Similarly, Philippa Sleeman et al. found that high-fat diet protected pigs from post-cardiopulmonary bypass AKI[36]. On the other hand, several clinical investigations have indicated that kidney function is inversely related to circulating chemerin levels in CKD patients. For example, the serum chemerin levels in stages 3 and 4 CKD patients were higher than in the control group[37]. Following successful kidney transplantation, serum chemerin concentrations returned to normal levels, comparable to those of healthy controls[38]. Additionally, a negative correlation between serum chemerin levels and renal function was observed in another clinical investigation[39]. These findings suggest that chemerin might be a marker for CKD, and potentially a contributor to its development. However, no functional studies to date provided direct evidence supporting this hypothesis. Therefore, the precise role of chemerin in AKI and CKD, along with the underly mechanisms, remains unclear.

Chemerin is a cytokine primarily secreted by adipocytes and has therefor been classified as an adipokine, although it is also produced by other tissues, including the liver, uterus, ovary, testes, colon, and spleen in mice[40]. In the present study, we identified the expression of chemerin and its receptor CMKLR1 in the kidney, particularly in renal tubular epithelial cells, suggesting that chemerin may be involved in renal function through an autocrine pathway. Moreover, we observed a marked reduction in chemerin expression in the kidneys of I/R model mice. In TCMK-1 cells, chemerin expression also decreased following acute injury, such as exposure to H_2O_2. Most notably, serum chemerin levels in AKI patients were lower compared to healthy controls. These findings strongly suggest that chemerin plays a role in the progression of AKI. Chemerin-9, the active form of chemerin, consists of nine amino acids at the carboxy-terminal end[41,42]. To further explore chemerin's role, we treated I/R mice with recombinant chemerin-9 via tail vein injection. Remarkably, we found that chemerin-9 treatment significantly attenuated renal injury induced by I/R. Overall, these findings indicate that chemerin may play a protective role in renal function during AKI, and they also provide direct evidences supporting the "obesity paradox in renal function" mentioned earlier.

Growing evidence indicates that ferroptosis plays a key role in the pathogenesis of AKI, and inhibiting ferroptosis may be an effective strategy for treating AKI[7,43,44]. Additionally, chemerin has been shown to enhance the anti-ferroptosis capacity of cancer cells[16]. Notably, renal tubular cells are particularly vulnerable to various harmful stimuli, leading to severe dysfunction and, ultimately, renal failure in I/R-associated AKI[45]. Consistent with these observations, several strategies targeting ferroptosis inhibition in renal tubular cells have yielded positive outcomes[7,44,46,47]. Based on these findings, we hypothesized that chemerin attenuates AKI by inhibiting

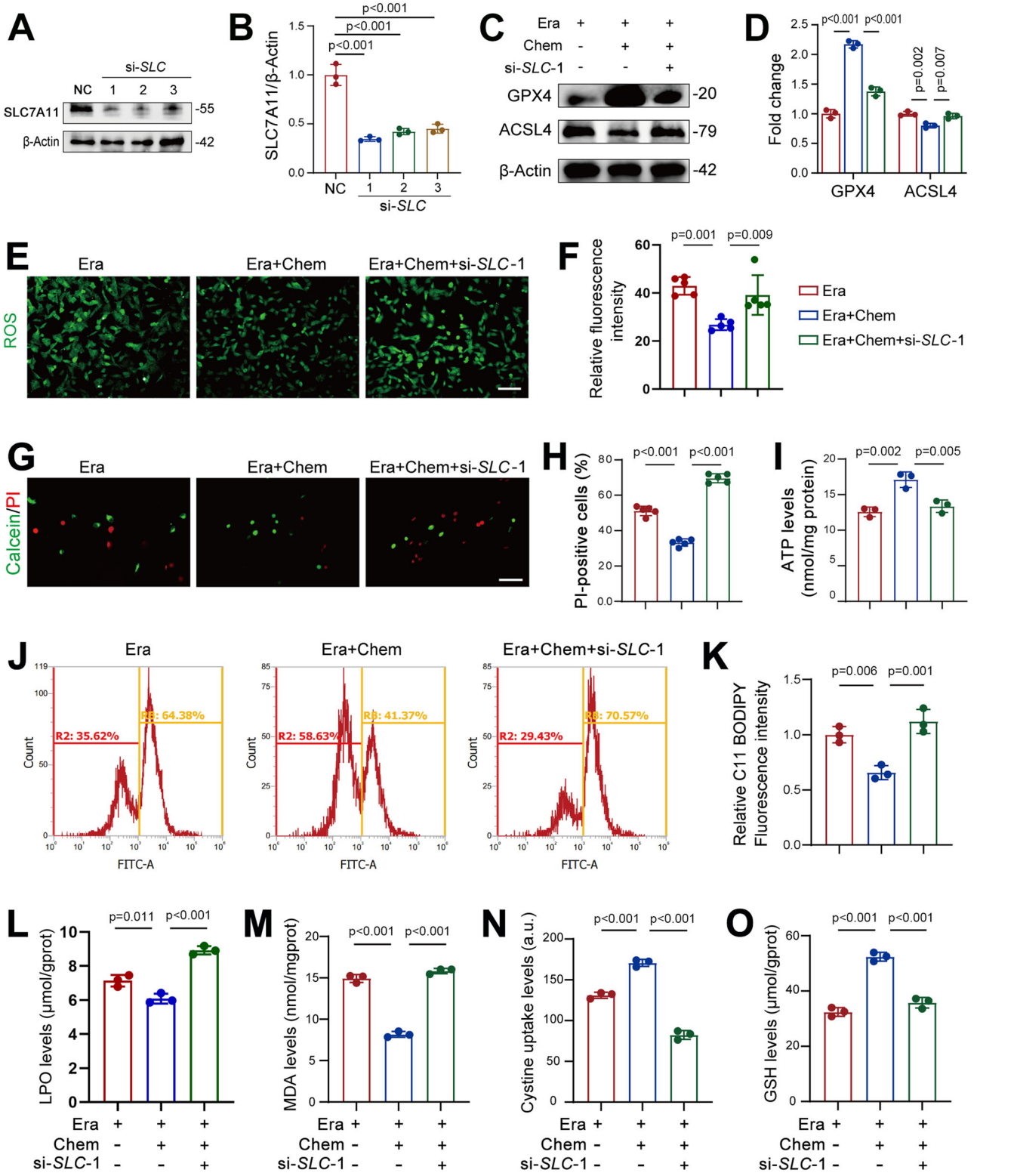

ferroptosis in renal tubular cells. This hypothesis was supported by our data, which showed that chemerin knockdown exacerbated erastin-induced cell injury, a detrimental effect that was largely mitigated by the application of recombinant chemerin.

SLC7A11 is a transmembrane protein that plays a critical role in cysteine production and GSH biosynthesis by transporting extracellular cystine into cells. By maintaining intracellular GSH levels, SLC7A11 helps defend against oxidative stress and ferroptosis[48–50]. In this study, we found that chemerin treatment upregulated SLC7A11 expression in I/R injured kidneys and erastin-treated TCMK-1 cells, suggesting that the renal protective effects of chemerin may be mediated through the enhancement of SLC7A11 in renal tubular cells. Furthermore, knockdown of SLC7A11 exacerbated erastin-induced ferroptosis in TCMK-1 cells, an effect that was reversed by chemerin administration. These results further support the notion that chemerin mitigates renal dysfunction in I/R model mice by promoting SLC7A11 expression in renal tubular cells. NRF2 is a key

Fig. 6 | Chemerin mitigates ferroptosis by upregulating SLC7A11 expression in renal tubular epithelial cells. **A** Knockdown of SLC7A11 by siRNA. TCMK-1 cells were transfected with siRNA targeting *Slc7a11* (si-*SLC*). Seventy-two hours post-transfection, SLC7A11 expression was analyzed by western blot, with β-Actin used as a loading control. $n = 3$ (independent experiments). **B** Quantification of SLC7A11 expression from the western blots shown in (**A**). **C** SLC7A11 knockdown reverses the changes in GPX4 and ACSL4 induced by chemerin. TCMK-1 cells were transfected with si-*SLC* for 48 h, then treated with erastin (Era, 5 μM) and the recombinant chemerin (20 ng/ml) for an additional 24 h. Protein expression was analyzed by western blot, with β-Actin used as a loading control. $n = 3$ (independent experiments). **D** Quantification of GPX4 and SLC7A11 from the western blots shown in (**C**). **E** Reactive oxygen species (ROS) levels. Cell treatments were as described in (**C**). $n = 5$ (independent experiments). Scale bar = 50 μm. **F** Quantified ROS levels from the images shown in (**E**). **G** Calcein/PI staining. Cell treatments were as described in (**C**). $n = 5$ (independent experiments). Scale bar = 50 μm. **H** Quantified PI-positive cells from the images shown in (**G**). **I** ATP levels. Cell treatments were as described in (**C**). $n = 3$ (independent experiments). **J** Lipid peroxidation. Oxidized lipids were captured by using C11 BODIPY and assayed by flow cytometry. Cell treatments were as described in (**C**). $n = 3$ (independent experiments). **K** Quantified lipid peroxidation from the images shown in (**J**). Lipid hydroperoxide (LPO; **L**), malondialdehyde (MDA; **M**), cystine uptake (**N**), and GSH levels (**O**). Cell treatments were as described in (**C**). $n = 3$ (independent experiments). Data are presented as the mean ± SD. $^{*}p < 0.05$, $^{**}p < 0.01$, $^{***}p < 0.001$, by one-way ANOVA with Tukey's multiple comparison test.

transcriptional factor that regulates SLC7A11 expression in various cell types, including brain vascular endothelial cells, renal cell carcinoma, colorectal cancer cells[30–32]. Additionally, NRF2 is a downstream target of AMPK[51–53]. Specifically, AMPK phosphorylates NRF2, promoting its nuclear translocation, where it acts as a transcriptional factor to activate the expression of downstream genes. Based on these observations, we hypothesized that chemerin increases SLC7A11 expression in renal tubular cells by activating the AMPK/NRF2 signaling pathway. Indeed, our data showed that chemerin induced phosphorylation of AMPK and NRF2 in TCMK-1 cells, leading to the nuclear translocation of p-NRF2, which in turn activated SLC7A11 expression. Pharmacological interventions with AMPK and NRF2 inhibitors further validated these findings. Consistent with our results, chemerin has been shown to activate the AMPK/NRF2 pathway to ameliorate neuronal apoptosis and atherosclerosis[54,55]. Moreover, NRF2-deficient mice have been reported to be more susceptible to AKI induced renal failure[56], further supporting our conclusions.

In conclusion, this study unveiled a role of chemerin, an adipokine, in renal pathophysiology. We found that chemerin expression was inversely correlated with the progression of AKI, and its administration significantly attenuated renal dysfunction in I/R model mice. Mechanistically, chemerin activated AMPK, which in turn promoted the nuclear translocation of NRF2. Once in the nucleus, NRF2 acted as a transcriptional factor to upregulate SLC7A11 expression in renal tubular cells. This led to increased cystine uptake and enhanced GSH biosynthesis, thereby boosting the cells' capacity to resist AKI-associated ferroptosis. These findings suggest that chemerin may hold significant therapeutic potential for the treatment of AKI and other ferroptosis-related conditions. Moreover, this study highlights the crosstalk between white adipose tissue and the kidney, providing a theoretical foundation for understanding the "adiposity paradox".

Methods

Animal models

Male C57BL/6 mice (21 ± 3 g; 8–12 weeks) were obtained from the Center of Laboratory Animals at Nantong University. The mice were randomly assigned to different experimental groups (n = 6). The I/R model was established using a previously described protocol[57]. In brief, after anesthetization, the mice underwent a skin incision, and the fascia was opened to expose the kidneys. Bilateral renal ischemia was induced by occluding the renal hilum on both sides using microvascular clips for 45 min. Following the procedure, the muscle and skin were sutured. C-terminal peptide of full-length mouse chemerin (chemerin-9; TOCRIS, Catalog#7117) was administered via tail vein injection at a dosage of 300 mg/kg. In the sham group, only a mock laparotomy was performed, and saline was injected via the tail vein. In other AKI animal models, cisplatin (232120, Sigma-Aldrich) or lipopolysaccharides (LPS; L2630, Sigma-Aldrich) was administrated to mice by intraperitoneal injection (i.p.) at a dosage of 20 mg/kg or 10 mg/kg, respectively[58,59]. Mice were sacrificed at different time points (6, 12, 24 and 72 h) post-ischemia, and blood and kidney samples were collected for further analysis. We have complied with all relevant ethical regulations for animal use.

Human blood specimens

The peripheral blood samples from healthy controls and CKD patients were obtained from the Affiliated Hospital of Nantong University. Human sample collection for research was conducted in accordance with the recognized ethical guideline of Declaration of Helsinki. All ethical regulations relevant to human research participants were followed.

Ethics approval

Animal procedures were approved by the Animal Experimentation Ethics Committee of the Nantong University (SYXK [SU] 2017-0046). Human blood analysis was approved by the Institutional Research Ethics Committee of Affiliated Hospital of Nantong University (2022-138-01).

Measurement of serum creatinine, blood urea nitrogen (BUN)

Serum creatinine and BUN were measured with a creatinine assay kit (JianCheng, C011-2-1, Nanjing, China) and a BUN assay kit (JianCheng, C013-2-1, Nanjing, China), respectively, using the manufacturer's instructions.

Chemerin assay

Mouse serum chemerin levels were assayed using an ELISA kit (SuKeMei, MK5855B, China) following the provided protocol. Human serum chemerin levels were analyzed using a human-specific ELISA kit (SuKeMei, MK3694B, China).

Transmission electron microscopy (TEM)

Kidney sections were fixed in electron microscope fixative (Servicebio, G1102, China) for 24 h. The samples were then incubated in 1% osmium acid for 2 h at room temperature, followed by dehydrated using a gradient ethanol series. Afterward, the samples were embedded in epoxy resin and sectioned into 70 nm slices. The samples were subsequently stained with 3% citrate−uranyl acetate. Mitochondrial structures were examined using a transmission electron microscope (JEOL, JEM-200CXCo, Japan).

Hematoxylin and eosin (H&E) staining

Tissue samples were fixed in formalin, embedded in paraffin and sectioned into 5 μm thick slices. The sections were then stained with hematoxylin and eosin (H&E) staining. Images were captured using a microscope (Olympus, IX71, Japan). An established grading scale of 0–4 was employed to assess histopathology of I/R-induced injury[60].

Cell culture and treatments

TCMK-1 cells were obtained from the American Type Culture Collection (ATCC; CCL-139). Cells were cultured in a 1:1 mixture of DMEM and F12 medium, supplemented with 10% fetal bovine serum (FBS) and 1% penicillin/streptomycin (P/S). Cells were cultured in a humidified chamber with 5% CO_2 at 37°C. Ferroptosis was induced by treating the cells with 10 μM erastin (MedChemExpress, HY-15763, USA) for 24 h. Acute injury was induced by treating the cells with 100 μM H_2O_2 for 24 h. To assess the protective effects of chemerin, cells were treated with 20 ng/ml mouse recombinant chemerin (HY-P75554, MedChemExpress) for 24 h.

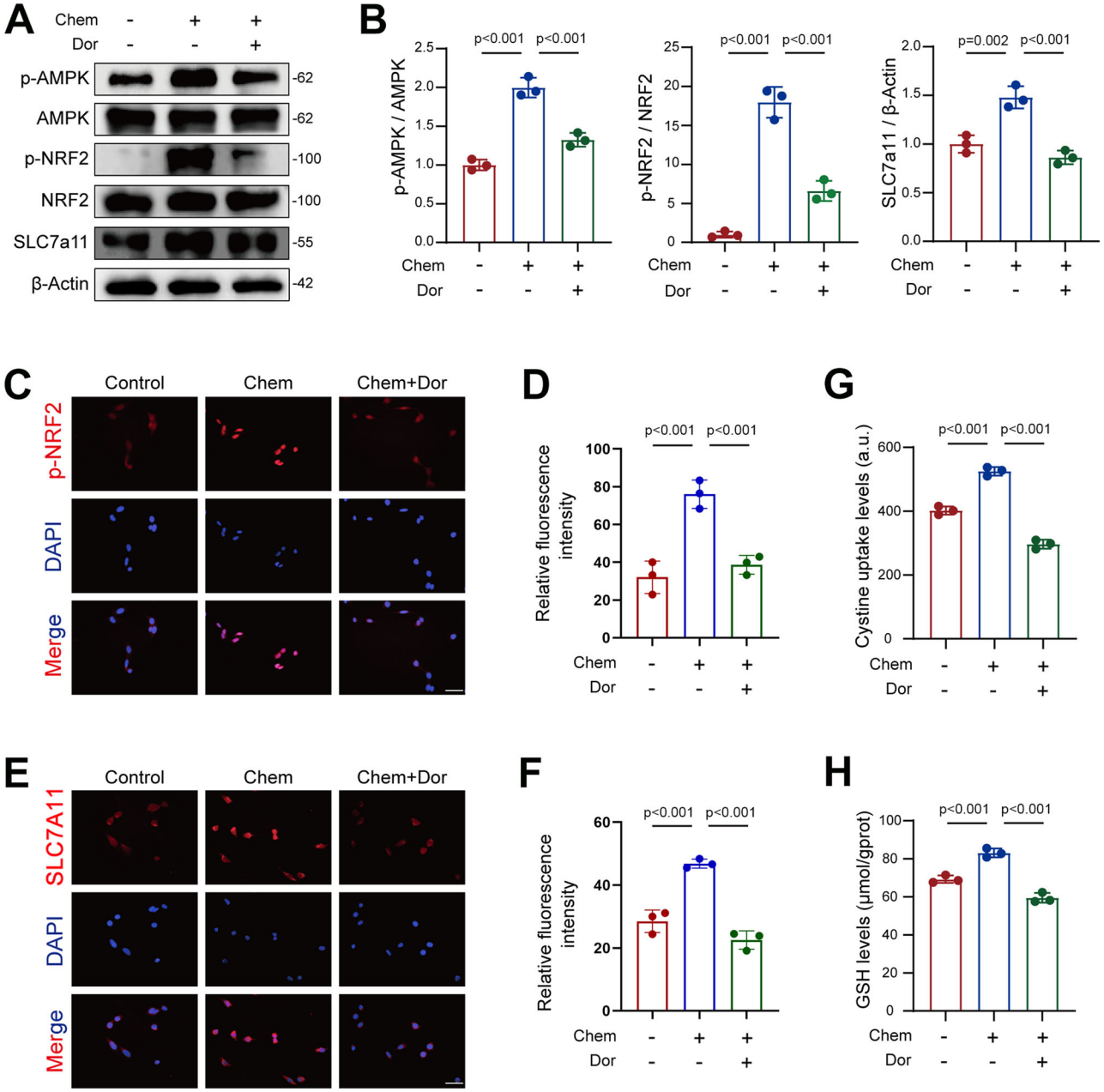

Fig. 7 | Chemerin alleviates ferroptosis through the AMPK/NRF2 pathway in renal tubular epithelial cells. A Chemerin activates NRF2 and SLC7A11 in an AMPK-dependent manner. TCMK-1 cells were treated with the recombinant chemerin (20 ng/ml) and dorsomorphin (Dor, 5 μM) for 24 h. Protein levels were analyzed by western blot, with β-Actin used a loading control. $n = 3$ (independent experiments). **B** Quantified data from the western blots shown in (**A**). **C–F** Representative immunofluorescence staining images for phosphorylated NRF2 (p-NRF2; **C**) and SLC7A11 (**E**). The corresponding relative immunofluorescence intensities are shown in (**D**) and (**F**), respectively. Cell treatments were as descried in (**A**). $n = 3$ (independent experiments). Scale bar = 50 μm. Cystine uptake (**G**) and GSH levels (**H**) in TCMK-1 cells treated with recombinant chemerin and Dor. Cell treatments were as described as in (**A**). $n = 3$ (independent experiments). Data are presented as the mean ± SD. $^{**}p < 0.01$ and $^{***}p < 0.001$, by one-way ANOVA with Tukey's multiple comparison test.

Western blot analysis

Western blot analysis was performed with the previously described procedures[61]. Briefly, kidney tissues and TCMK-1 cells were lysed in RIPA lysis buffer (Beyotime, P0013B, Shanghai, China), and protein concentration were measured using a protein assay kit (Beyotime P0011, Shanghai, China). Protein samples were then separated on 8-15% SDS-PAGE gels and transferred onto PVDF membranes (Millipore, IPVH00010, ISEQ00010, USA). The membranes were incubated with primary antibodies at 4°C overnight, followed by incubation with secondary antibodies (Proteintech, SA00001-1, SA00001-2, USA) for 1 h at room temperature. The primary antibodies used in this study include: Chemerin (Abcam, ab103153, USA; 1:1000), CMKLR1 (Santa Cruz Biotechnology, SC-398769, USA; 1:1000), TNFα (Proteintech, 60291-1-Ig, USA; 1:1000), IL-6 (Proteintech, 21865-1-AP, USA; 1:1000), ACSL4 (Proteintech, 22401-1-AP, USA; 1:1000), GPX4 (Proteintech, 67763-1-Ig, USA; 1:1000), SLC7A11 (Abcam, ab175186, USA; 1:1000), p-NRF2 (Invitrogen, PA5-67520, USA; 1:1000), Lamin A/C (Cell Signaling Technology, 4777, USA; 1:1000), p-AMPK (Cell Signaling Technology, 2535 T, USA; 1:1000), AMPK (Proteintech, 10929-2-AP, USA; 1:1000), β-Actin (Proteintech, 66009-1-Ig, USA; 1:10000), GAPDH (Proteintech, 60004-1-Ig, USA; 1:10000), α-Tubulin (Proteintech, 11224-1-AP, USA; 1:10000).

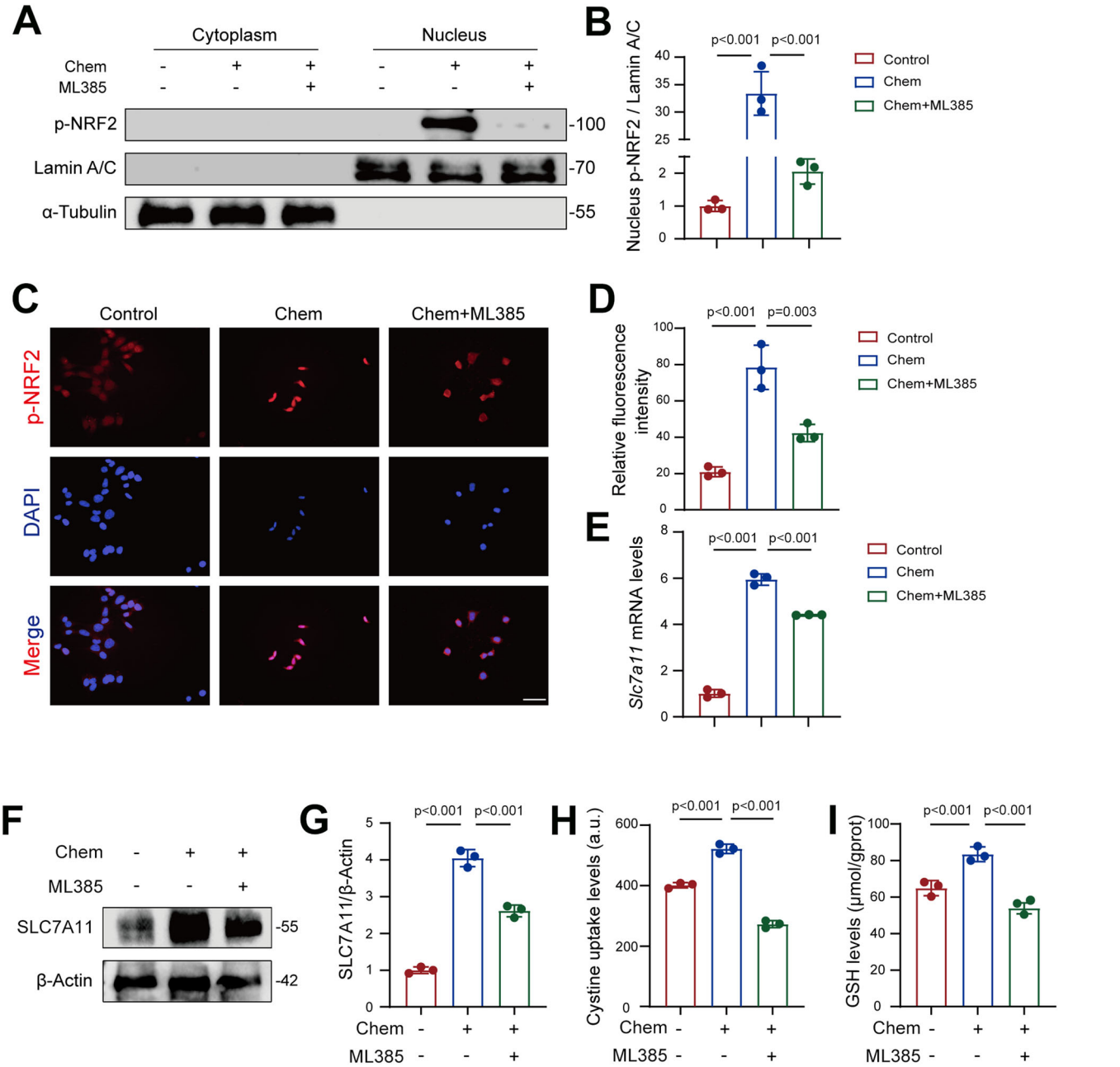

Fig. 8 | Chemerin promotes NRF2 nuclear translocation to induce SLC7A11 transcription in renal tubular epithelial cells. A NRF2 inhibition prevents chemerin-induced nuclear translocation of NRF2. TCMK-1 cells were treated with recombinant chemerin (20 ng/ml) and NRF2 inhibitor ML385 (10 μM) for 24 h. Cytoplasmic and nuclear protein samples were prepared for western blot analysis. Lamin A/C was used as a loading control for nuclear proteins, and α-Tubulin was used as a loading control for cytoplasmic proteins. $n = 3$ (independent experiments). **B** Quantification of NRF2 levels from the western blots shown in (**A**). **C** Representative immunofluorescence staining images of phosphorylated NRF2 (p-NRF2). Cell treatments were as described in (**A**). $n = 3$ (independent experiments). Scale bar = 50 μm. **D** Relative fluorescence intensity of p-NRF2 as shown in (**C**). **E** mRNA levels of SLC7A11 in TCMK-1 cells treated with the recombinant chemerin and ML385. Cell treatments were as described in (**A**). $n = 3$ (independent experiments). **F** Western blot analysis of SLC7A11 in TCMK-1 cells treated with Chemerin and ML385. Cell treatments were as described in (**A**). β-Actin was used a loading control. $n = 3$ (independent experiments). **G** Quantification of SLC7A11 from the western blots shown in (**F**). Cystine uptake (**H**) and GSH levels (**I**). Cell treatments were as described in (**A**). $n = 3$ (independent experiments). Data are presented as the mean ± SD. $^{**}p < 0.01$ and $^{***}p < 0.001$, by one-way ANOVA with Tukey's multiple comparison test.

Quantitative real-time PCR (qRT-PCR)

Total RNA was extracted from tissues or cells using RNA Extraction Reagent (Vazyme, R401-01, China), which was then reversely transcribed into cDNA using a kit (Vazyme, R333-01, Nanjing, China). The qRT-PCR was performed using SYBR qPCR Master Mix (Vazyme, R401-01, Q712-02, China) with a Studio Q5 apparatus (ABI, A28134, USA). Primer sequences used for qRT-PCR are: *Chemerin* (mouse) 5'-AAT TTA AGC TCC AGC AGA CCA AC-3' (forward), 5'-ATC CGG CCT AGA ATT TTA CCC TT-3' (reverse); *CMKLR1* (mouse) 5'-TCC TGT TCA ACA TCT TTT TGC C-3' (forward), 5'-CAA GAA GTT GCT GAT CTT GCA C-3' (reverse); *SLC7A11* (mouse) 5'- AAT ACG GAG CCT TCC ACG AG-3' (forward), 5'-ACT GTT CGG TCG TGA CTT CC-3' (reverse); *GPX4* (mouse) 5'- GAC GCC AAA GTC CTA GGA AAC-3' (forward), 5'-CCG GGT TGA AAG GTT CAG GA-3' (reverse); *GAPDH* (mouse) 5'- CCC TTA AGA GGG

ATG CTG CC-3' (forward), 5'-ACT GTG CCG TTG AAT TTG CC-3' (reverse). The relative gene expression was normalized to *GAPDH*.

Intracellular ROS assay

A fluorescent probe, namely dichlorodihydrofluorescein diacetate (DCFH-DA; Beyotime, S0033S, Shanghai, China), was used for detecting ROS in cells. Photographs were acquired with a microscope (Olympus, IX71, Japan). The stained areas with positive signals were quantified using the Image J software.

Detection of MDA, GSH and LPO levels

Approximately 10 mg of kidney tissue or 1×10^6 cells were collected, washed with cold PBS, and then homogenized. MDA concentrations were measured using a commercial kit (Beyotime, S0131S, Shanghai, China). GSH levels were assessed with a reduced glutathione (GSH) assay kit (JianCheng, A006-2-1, Nanjing, China), and LPO levels were determined using a lipid peroxidation assay kit (JianCheng, A106-1-1, Nanjing, China).

Knockdown of Chemerin and SLC7A11

Chemerin gene knockdown was performed in TCMK-1 cells by small interfering RNAs (siRNAs). The siRNAs targeting *Chemerin* (si-*Chem*) and *Slc7a11* (si-*SLC*) were synthesized at GenePharma (Shanghai, China) with the sequences of UGA AGA AGU GCU CUU CUC ATT (si-*Chem*-1), ACC UUU GUG AGG UUG GAA UTT (si-*Chem*-2), ACA AUC AAA CCA AAC GGG ATT (si-*Chem*-3); and GGU GGA ACU GCU CGU AAU ATT (si-*SLC*-1), CUG CAU AUU AUC UCU UCA U (si-*SLC*-2), CCU GUC CUA UGC AGA AUU ATT (si-*SLC*-3). The synthesized siRNAs were transfected in TCMK-1 cells using a FECT CP transfection kit (Ribobio, C10511-05, China).

Immunofluorescence analysis

Kidney tissue slices and cells were fixed in 4% PFA for 30 min at room temperature, followed by permeabilization with 0.2% Triton X-100 for 10 min. Samples were then blocked with 5% BSA for 30 min at room temperature. After blocking, samples were incubated with the primary antibodies overnight at 4°C. The primary antibodies used were: Chemerin (sc-373797; Santa Cruz Biotechnology, USA; 1:500), CMKLR1 (SC-398769; Santa Cruz Biotechnology, USA; 1:500), TNFα (60291-1-Ig; Proteintech, USA; 1:500), IL-6 (21865-1-AP; Proteintech, USA; 1:500), ACSL4 (22401-1-AP; Proteintech, USA; 1:500), GPX4 (67763-1-Ig; Proteintech, USA; 1:500), SLC7A11 (ab175186; Abcam, USA; 1:500), p-NRF2 (PA5-67520; Invitrogen, USA; 1:200), NRF2 (80593-1-RR; Proteintech, USA; 1:500), AQP1 (ab168387; Abcam, USA; 1:500), and Cytokeratin 19 (CK19; 60187-lg; Proteintech, USA; 1:500). Subsequently, samples were incubated with second antibodies conjugated with CY5 or 488 for 1 h at room temperature. Nuclei were stained with DAPI (Servicebio, G1012, China) for 10 min at room temperature. Images were captured using a microscope (Olympus, IX71, Japan), and quantification was performed using ImageJ software.

Cytoplasmic and nuclear protein extraction

Cytoplasmic and nuclear protein samples were extracted using a commercial kit (Beyotime, P0027, Shanghai, China). Briefly, cells were thoroughly mixed with reagent A and kept on ice. After adding reagent B, the cells were homogenized on ice. The mixture was then centrifuged at 12,000 g for 5 min at 4°C, and the supernatant was collected as the cytoplasmic protein sample. The remaining pellet was resuspended in the nuclear protein extraction reagent. After further homogenization on ice, the samples were centrifuged at 12,000 g for 10 min, and the supernatants were collected as nuclear protein fractions.

Cystine uptake assay

Cystine uptake was assayed using a cystine uptake assay kit (Dojindo Laboratories, UP05, Japan). Fluorescence was detected using a microplate reader (Tecan, Spark®, Switzerland).

RNA-Seq

Kidney tissues from I/R and Chemerin-9 treated I/R mice were prepared for RNA-seq analysis at Servicebio (Wuhan, China). An Illumina Novaseq6000 platform was applied to sequence the libraries. Subsequently, differentially expressed genes were listed and analyzed with the Kyoto Encyclopedia of Genes (KEGG) and Gene Ontology (GO) enrichment. Three repetitions per group were used for these analyses.

Chemerin, IL-6, and TNFα assays

RIPA-extracted cellular proteins and mouse serum were used for analyzing IL-6 and TNFα levels. Chemerin, IL-6, and TNFα levels were measured, respectively, using a mouse chemerin ELISA kit (MK5855B; MeiKe, Nanjing, China), a mouse TNFα ELISA kit (MK2868B; MeiKe, Nanjing, China), and a mouse IL-6 ELISA kit (MK5737B; MeiKe, Nanjing, China) according to the manufacturer's instructions. Human serum chemerin levels were measured using a human ELISA kit (MK3694B; MeiKe, Nanjing, China) according to the manufacturer's instructions.

Periodic acid-Schiff stain (PAS) staining

Kidney samples were fixed in formalin, embedded in paraffin and sectioned to 5 μm thick sections. The slices were stained with PAS. Images were collected by a microscope (Olympus, IX71, Japan). An established grading scale of 0–4 was used to evaluate histopathology of I/R-induced injury[60].

Calcein-AM/PI staining

Calcein-AM/PI double staining kit (Solarbio, CA1630, China) was used to evaluate cell death in vitro. After treatment, TCMK-1 cells were washed with PBS gently and stained with calcein AM and PI for 30 min. Photographs were acquired with a microscope (Olympus, IX71, Japan). The positively stained areas were quantified using the ImageJ software.

ATP assay

ATP levels were determined using an enhanced ATP assay kit (S0026; Beyotime, Shanghai, China) according to the manufacturer's protocol. Briefly, after treatments, TCMK-1 cells were collected for metabolite extraction. ATP concentration was measured using a luminometer relative to the reference ATP solution.

C11 BODIPY staining

TCMK-1 cells were incubated with 1 μM C11 BODIPY 581/591 lipid peroxidation probe (RM02821; Abclonal, Wuhan, China) for 30 min at 37°C in the dark. The signal corresponding to 510 nm was measured using a flow cytometer (BD FACSCelesta, Multicolor Flow Cytometer) at excitation with a 488 nm laser. Histograms were made separately from the channel signals of the FACS to quantify the proportion of lipid peroxidation cells.

Statistics and reproducibility

All data were expressed as mean ± standard deviation (SD). The sample sizes and number of replicates were defined in each figure legend. Intergroup comparisons were done with unpaired Student's *t* test, and multigroup comparisons were done with one-way ANOVA with Tukey's multiple comparison test. GraphPad Prism 9.0 software was employed for all analyses. $P < 0.05$ was considered as statistical significance.

Data availability

Source data used for generating the plots in the main figures are shown in Supplementary Data 1. RNA-Seq data have been deposited to the GEO (accessing number GSE283126). Uncropped and unedited blots are shown in Supplementary Figs. 9–12. Additional information and reagents are available from the corresponding author upon reasonable request.

Received: 27 March 2024; Accepted: 6 December 2024;
Published online: 19 December 2024

References

1. See, E. J. et al. Long-term risk of adverse outcomes after acute kidney injury: a systematic review and meta-analysis of cohort studies using consensus definitions of exposure. *Kidney Int.* **95**, 160–172 (2019).
2. Poston, J. T. & Koyner, J. L. Sepsis associated acute kidney injury. *BMJ* **364**, k4891 (2019).
3. Bucaloiu, I. D. et al. Increased risk of death and de novo chronic kidney disease following reversible acute kidney injury. *Kidney Int.* **81**, 477–485 (2012).
4. Schetz, M., Gunst, J., De Vlieger, G. & Van den Berghe, G. Recovery from AKI in the critically ill: potential confounders in the evaluation. *Intensive Care Med.* **41**, 1648–1657 (2015).
5. Coca, S. G., Singanamala, S. & Parikh, C. R. Chronic kidney disease after acute kidney injury: a systematic review and meta-analysis. *Kidney Int.* **81**, 442–448 (2012).
6. Pickkers, P. et al. The intensive care medicine agenda on acute kidney injury. *Intensive Care Med.* **43**, 1198–1209 (2017).
7. Chu, L. K. et al. Autophagy of OTUD5 destabilizes GPX4 to confer ferroptosis-dependent kidney injury. *Nat. Commun.* **14**, 8393 (2023).
8. Linkermann, A. Nonapoptotic cell death in acute kidney injury and transplantation. *Kidney Int.* **89**, 46–57 (2016).
9. Sakashita, M. & Nangaku, M. Multi-omics studies reveal genes critical for AKI and ferroptosis. *Kidney Int.* **101**, 665–667 (2022).
10. Guo, R. et al. The road from AKI to CKD: molecular mechanisms and therapeutic targets of ferroptosis. *Cell Death Dis.* **14**, 426 (2023).
11. Sanz, A. B., Sanchez-Nino, M. D., Ramos, A. M. & Ortiz, A. Regulated cell death pathways in kidney disease. *Nat. Rev. Nephrol.* **19**, 281–299 (2023).
12. Helfer, G. & Wu, Q. F. Chemerin: a multifaceted adipokine involved in metabolic disorders. *J. Endocrinol.* **238**, R79–r94 (2018).
13. Bondue, B., Wittamer, V. & Parmentier, M. Chemerin and its receptors in leukocyte trafficking, inflammation and metabolism. *Cytokine Growth Factor Rev.* **22**, 331–338 (2011).
14. Carracedo, M. et al. Chemerin inhibits vascular calcification through ChemR23 and is associated with lower coronary calcium in chronic kidney disease. *J. Intern. Med.* **286**, 449–457 (2019).
15. Zhao, K. et al. Variants in the RARRES2 gene are associated with serum chemerin and increase the risk of diabetic kidney disease in type 2 diabetes. *Int. J. Biol. Macromol.* **165**, 1574–1580 (2020).
16. Tan, S. K. et al. Obesity-dependent adipokine chemerin suppresses fatty acid oxidation to confer ferroptosis resistance. *Cancer Discov.* **11**, 2072–2093 (2021).
17. Berndt, C. et al. Ferroptosis in health and disease. *Redox Biol.* **75**, 103211 (2024).
18. Lin, Q. et al. PINK1-parkin pathway of mitophagy protects against contrast-induced acute kidney injury via decreasing mitochondrial ROS and NLRP3 inflammasome activation. *Redox Biol.* **26**, 101254 (2019).
19. Chen, D. et al. NRF2 is a major target of ARF in p53-independent tumor suppression. *Mol. Cell* **68**, 224–232 e224 (2017).
20. Zhang, Y. et al. BAP1 links metabolic regulation of ferroptosis to tumour suppression. *Nat. Cell Biol.* **20**, 1181–1192 (2018).
21. Wang, Y. et al. Epigenetic regulation of ferroptosis by H2B monoubiquitination and p53. *EMBO Rep.* **20**, e47563 (2019).
22. Kim, M. J. et al. Kaempferol stimulation of autophagy regulates the ferroptosis under the oxidative stress as mediated with AMP-activated protein kinase. *Free Radic. Biol. Med.* **208**, 630–642 (2023).
23. Kong, P. et al. Ferroptosis triggered by STAT1- IRF1-ACSL4 pathway was involved in radiation-induced intestinal injury. *Redox Biol.* **66**, 102857 (2023).
24. Lee, H. et al. Energy-stress-mediated AMPK activation inhibits ferroptosis. *Nat. Cell Biol.* **22**, 225–234 (2020).
25. Wu, W. et al. IL-10 protects against OPC ferroptosis by regulating lipid reactive oxygen species levels post stroke. *Redox Biol.* **69**, 102982 (2023).
26. Lu, Q. et al. Empagliflozin attenuates the renal tubular ferroptosis in diabetic kidney disease through AMPK/NRF2 pathway. *Free Radic. Biol. Med.* **195**, 89–102 (2023).
27. El-Horany, H. E. et al. Empagliflozin ameliorates bleomycin-induced pulmonary fibrosis in rats by modulating Sesn2/AMPK/Nrf2 signaling and targeting ferroptosis and autophagy. *Int. J. Mol. Sci.* **24**, 9481 (2023).
28. Liu, Y. et al. Vitamin C sensitizes pancreatic cancer cells to erastin-induced ferroptosis by activating the AMPK/Nrf2/HMOX1 pathway. *Oxid. Med. Cell Longev.* **2022**, 5361241 (2022).
29. He, F., Ru, X. & Wen, T. NRF2, a transcription factor for stress response and beyond. *Int. J. Mol. Sci.* **21**, 4777 (2020).
30. Li, P. et al. Protective effect of compound Tongluo Decoction on brain vascular endothelial cells after ischemia-reperfusion by inhibition of ferroptosis through regulating Nrf2/ARE/SLC7A11 signaling pathway. *Adv. Biol.* **8**, e2300416 (2023).
31. Chang, K. et al. DPP9 stabilizes NRF2 to suppress ferroptosis and induce sorafenib resistance in clear cell renal cell carcinoma. *Cancer Res.* **83**, 3940–3955 (2023).
32. Wu, W. et al. Non-canonical role of UCKL1 on ferroptosis defence in colorectal cancer. *EBioMedicine* **93**, 104650 (2023).
33. Sakers, A., De Siqueira, M. K., Seale, P. & Villanueva, C. J. Adipose-tissue plasticity in health and disease. *Cell* **185**, 419–446 (2022).
34. Zhou, D., Wang, C., Lin, Q. & Li, T. The obesity paradox for survivors of critically ill patients. *Crit. Care* **26**, 198 (2022).
35. Stenvinkel, P. et al. Inflammation modifies the paradoxical association between body mass index and mortality in hemodialysis patients. *J. Am. Soc. Nephrol.* **27**, 1479–1486 (2016).
36. Sleeman, P. et al. High fat feeding promotes obesity and renal inflammation and protects against post cardiopulmonary bypass acute kidney injury in swine. *Crit. Care* **17**, R262 (2013).
37. Blaszak, J. et al. High serum chemerin level in CKD patients is related to kidney function, but not to its adipose tissue overproduction. *Ren. Fail* **37**, 1033–1038 (2015).
38. Rutkowski, P. et al. Decrease of serum chemerin concentration in patients with end stage renal disease after successful kidney transplantation. *Regul. Pept.* **173**, 55–59 (2012).
39. Zylla, S. et al. Serum chemerin levels are inversely associated with renal function in a general population. *Clin. Endocrinol.* **88**, 146–153 (2018).
40. Luangsay, S. et al. Mouse ChemR23 is expressed in dendritic cell subsets and macrophages, and mediates an anti-inflammatory activity of chemerin in a lung disease model. *J. Immunol.* **183**, 6489–6499 (2009).
41. Fischer, T. F. et al. Cyclic analogues of the chemerin C-terminus mimic a loop conformation essential for activating the chemokine-like receptor 1. *J. Med. Chem.* **64**, 3048–3058 (2021).
42. Sato, K. et al. Chemerin-9, a potent agonist of chemerin receptor (ChemR23), prevents atherogenesis. *Clin. Sci.* **133**, 1779–1796 (2019).
43. Hosohata, K., Harnsirikarn, T. & Chokesuwattanaskul, S. Ferroptosis: a potential therapeutic target in acute kidney injury. *Int. J. Mol. Sci.* **23**, 6583 (2022).
44. Cai, F. et al. Sulfide:quinone oxidoreductase alleviates ferroptosis in acute kidney injury via ameliorating mitochondrial dysfunction of renal tubular epithelial cells. *Redox Biol.* **69**, 102973 (2023).
45. Doyle, J. F. & Forni, L. G. Acute kidney injury: short-term and long-term effects. *Crit. Care* **20**, 188 (2016).
46. Zhong, D. et al. Targeting mPGES-2 to protect against acute kidney injury via inhibition of ferroptosis dependent on p53. *Cell Death Dis.* **14**, 710 (2023).
47. Tang, Z., Wang, Y., Liu, Y. & Li, C. Salidroside inhibits renal ischemia/reperfusion injury-induced ferroptosis by the PI3K/AKT signaling pathway. *Exp. Ther. Med.* **26**, 507 (2023).

48. Chen, Q. et al. SOCS2-enhanced ubiquitination of SLC7A11 promotes ferroptosis and radiosensitization in hepatocellular carcinoma. *Cell Death Differ.* **30**, 137–151 (2023).
49. He, F. et al. ATF4 suppresses hepatocarcinogenesis by inducing SLC7A11 (xCT) to block stress-related ferroptosis. *J. Hepatol.* **79**, 362–377 (2023).
50. Hong, T. et al. PARP inhibition promotes ferroptosis via repressing SLC7A11 and synergizes with ferroptosis inducers in BRCA-proficient ovarian cancer. *Redox Biol.* **42**, 101928 (2021).
51. Fathy, N., Farouk, S., Sayed, R. H. & Fahim, A. T. Ezetimibe ameliorates cisplatin-induced nephrotoxicity: a novel therapeutic approach via modulating AMPK/Nrf2/TXNIP signaling. *FASEB J.* **38**, e23382 (2024).
52. Kim, Y. E. et al. Forsythiaside A activates AMP-activated protein kinase and regulates oxidative stress via Nrf2 signaling. *Int. J. Mol. Sci.* **24**, 17033 (2023).
53. Liu, C., Rokavec, M., Huang, Z. & Hermeking, H. Salicylate induces AMPK and inhibits c-MYC to activate a NRF2/ARE/miR-34a/b/c cascade resulting in suppression of colorectal cancer metastasis. *Cell Death Dis.* **14**, 707 (2023).
54. Zhang, Y. et al. Chemerin reverses neurological impairments and ameliorates neuronal apoptosis through ChemR23/CAMKK2/AMPK pathway in neonatal hypoxic-ischemic encephalopathy. *Cell Death Dis.* **10**, 97 (2019).
55. Zhang, Y. et al. Chemerin suppresses neuroinflammation and improves neurological recovery via CaMKK2/AMPK/Nrf2 pathway after germinal matrix hemorrhage in neonatal rats. *Brain Behav. Immun.* **70**, 179–193 (2018).
56. Liu, M. et al. Transcription factor Nrf2 is protective during ischemic and nephrotoxic acute kidney injury in mice. *Kidney Int.* **76**, 277–285 (2009).
57. Jang, H. R. et al. Early exposure to germs modifies kidney damage and inflammation after experimental ischemia-reperfusion injury. *Am. J. Physiol. Ren. Physiol.* **297**, F1457–F1465 (2009).
58. Yang, L. et al. FFAR4 improves the senescence of tubular epithelial cells by AMPK/SirT3 signaling in acute kidney injury. *Signal Transduct. Target Ther.* **7**, 384 (2022).
59. Wang, Y. et al. The PINK1/PARK2/optineurin pathway of mitophagy is activated for protection in septic acute kidney injury. *Redox Biol.* **38**, 101767 (2021).
60. Leemans, J. C. et al. Renal-associated TLR2 mediates ischemia/reperfusion injury in the kidney. *J. Clin. Investig.* **115**, 2894–2903 (2005).
61. Yang, Y. et al. SIRT1 attenuates neuroinflammation by deacetylating HSPA4 in a mouse model of Parkinson's disease. *Biochim. Biophys. Acta Mol. Basis Dis.* **1868**, 166365 (2022).

Acknowledgements

This study was supported by a research grant from the Natural Science Foundation of China (82170750 and 82470762), the Special Scientific Research Project of Nantong Municipal Health Commission (MS2022007), the Foundation of Jiangsu Province Research Hospital (YJXYY202204-XKB13).

Author contributions

Yidan Ma: investigation, methodology, formal analysis, writing—original draft. Shengnan Fei: investigation, validation. Xu Chen, Yuanyuan Gui and Bing Zhou: resources, methodology; Tianya Xiang and Jianhang Liu: data curation. Kun Yue, Qingxin Li, and Wei Jiang: visualization, software. Wei Jiang: resources. Cheng Sun: project administration, writing—review & editing. Xinzhong Huang: conceptualization, supervision, funding acquisition. All authors read and approved the final manuscript.

Competing interests

The authors declare no competing interests.

Additional information

Supplementary information The online version contains supplementary material available at https://doi.org/10.1038/s42003-024-07377-x.

Correspondence and requests for materials should be addressed to Xinzhong Huang.

Peer review information *Communications Biology* thanks the anonymous reviewers for their contribution to the peer review of this work. Primary Handling Editors: Christopher Hine and Mengtan Xing. A peer review file is available.